Astron. Astrophys. 333, 251–263 (1998)

ASTRONOMY AND ASTROPHYSICS

The nitrogen spectra of Wolf-Rayet stars⋆

A grid of models and its application to the Galactic WN sample

W.-R. Hamann⋆⋆ and L. Koesterke⋆⋆

Lehrstuhl Astrophysik, Universität Potsdam, Am Neuen Palais 10, D-14469 Potsdam, Germany (wrh@astro.physik.uni-potsdam.de)

Received 2 October 1997 / Accepted 19 January 1998

Abstract. Adopting the "standard model" for Wolf-Rayet atmospheres, non-LTE radiation transfer calculations are performed which account for helium and nitrogen. Grids of theoretical models are presented for the whole relevant parameter range. The WN classification criteria are employed in order to identify the subtype domains, and inconsistencies are discussed. The (almost complete) sample of known Galactic WN stars is analyzed by comparing the observed spectra with the synthetic spectra of the grid models. This is the first time that nitrogen line analyses are performed for the whole WN sample, while previous comprehensive studies were restricted to helium models.

The obtained parameters roughly confirm the results from the previous helium analyses, as far as late subtypes (WNL) and early subtypes with strong lines (WNE-s) are concerned. For early subtypes with weak lines (WNE-w), however, the parameters are substantially revised. The hottest WN star, with a stellar (effective) temperature of 140 kK, is WR 2, which could not be analyzed previously from its helium lines due to the lack of He I. The other members of the WNE-w subgroup have stellar temperatures between 40 and 90 kK, thus populating the same temperature range as the strong-lined WNE-w, but with less dense winds.

The luminosities are revised according to the new parameters. Moreover, reddening corrections are newly determined form comparing IUE data with the UV model fluxes. The average luminosity is now $\log L/L_\odot = 5.5$ for WNE stars (both, strong and weak lined), and $\log L/L_\odot = 5.9$ for WNL (not significantly revised). The empirical minimum WN luminosity is $10^{5.0}\,L_\odot$, reducing former incompatibilities with predictions from evolutionary calculations. The ratio between mechanical and radiative momentum flow is slightly affected by the revisions, but remains much higher than unity: 9, 9 and 29 for the WNL, WNE-w and WNE-s subclass, respectively.

Key words: stars: fundamental parameters – Hertzsprung-Russell (HR) diagram – stars: mass loss – stars: Wolf-Rayet

1. Introduction

The quantitative analysis of Wolf-Rayet (WR) spectra requires adequate modelling of the non-LTE radiation transfer in spherically expanding stellar atmospheres. The first generations of such models, which became available with the work by Hillier (1987a.b) and by our group (e.g. Wessolowski et al. 1988), was restricted to the treatment of helium spectra. These models were considered to be adequate for WN-type atmospheres, which are predominantly composed of helium with only traces of nitrogen (remember that the WR stars are divided into a nitrogen – WN – and a carbon – WC – spectral sequence).

After these models have been tested in a few detailed analyses (e.g. Hamann et al. 1988), they were applied for coarse analyses of greater samples (30 Galactic WR stars: Schmutz et al. 1989; 19 WN stars in the Large Magellanic Cloud: Koesterke et al. 1991). In a comprehensive study (Hamann et al. 1993, in the following referred to as Paper I) we performed "coarse" analyses of the vast majority of the Galactic WN stars. Based on a grid of pure-helium models, the stellar parameters were determined from the measured equivalent widths of strategic helium lines. In a subsequent paper (Hamann et al. 1995a, hereafter Paper II) we completed the Galactic sample and performed individual calculations and profile fits for a couple of stars. Moreover, hydrogen was accounted for in these calculations in order to study the hydrogen abundances (in part of the WN atmospheres hydrogen is detectable, though more or less underabundant).

The WN star parameters which were obtained from these analyses imply far-reaching consequences, as they are not in line with standard evolutionary calculations, and are challenging the stellar wind modelling by the high mechanical-to-radiation momentum ratio. Therefore it is highly desirable to check the helium analyses with improved models which additionally account for nitrogen as the most abundant "metal" in WN atmospheres, exploiting the information carried with the nitrogen line spectrum.

Nitrogen has to be described by a very complex model atom, thus causing a much higher effort in the Non-LTE radiation

Send offprint requests to: W.-R. Hamann

⋆ Partly based on observations collected at the European Southern Observatory (ESO), La Silla, Chile, and on archival data from the International Ultraviolet Explorer (IUE)

⋆⋆ Visiting astronomers, German-Spanish Astronomical Center, Calar Alto, operated by the Max-Planck-Institut für Astronomie, Heidelberg, jointly with the Spanish National Commission for Astronomy

transfer calculations than hydrogen or helium. Corresponding models for WN stars were developed by Hillier (1988) and Hamann et al. (1994). These pilot studies both focused on an individual WN star (WR 6 and WR 136, respectively) of early subtype with strong lines (WNE-s, see Sect. 4.1 for the classification) and essentially confirmed the results of the previous pure-helium analyses. Crowther et al. (1994, 1995a,b) applied Hillier's code – accounting for nitrogen and even for carbon – to several late-type WN stars and again concluded that the previous pure-helium results are basically correct. However, a nitrogen study of three early-subtype WN stars with weak lines (i.e. WNE-w) led to substantially higher temperatures and luminosities (Crowther at al. 1995c).

In the present paper we now investigate the entire Galactic WN sample by means of the nitrogen spectra. For that purpose the whole relevant parameter range is covered by grids of theoretical models. The WN classification criteria are compared with the synthetic spectra, and the subtype domains are identified. For 62 (i.e. almost all) Galactic WN stars we establish their parameters by comparing the observed spectra with the synthetic spectra and selecting the best-fitting model from the grid.

The model calculations are characterized in the following section (Sect. 2). Subsequently, grids of models are presented and discussed (Sect. 3). These models are applied to analyze the Galactic WN stars from their nitrogen spectra as described in Sect. 4. The results are presented in the concluding section (Sect. 5).

2. The models

2.1. Basic assumptions and methods

The model calculations are of similar kind as described in previous papers (e.g. Hamann et al. 1994), and the reader is referred to these papers for more details and references. Only the basic assumptions and definitions are briefly repeated here.

A "standard" WR atmosphere is assumed to be expanding in a spherically-symmetric, homogeneous and stationary flow. With a given mass-loss rate $\dot{M}$, the density stratification and the velocity field $v(r)$ are related via the equation of continuity.

The velocity field is pre-specified from plausible ad-hoc assumptions. For the supersonic part we adopt the usual β-law (cf., e.g., Paper I, Eq. 1) with the terminal velocity v_∞ being a free parameter. The exponent β is set to unity throughout this work. In the subsonic region the velocity field is defined such that a hydrostatic density stratification is approached.

The "stellar radius" R_*, which is the inner boundary of our model atmosphere, corresponds per definition to a Rosseland optical depth of 20. In the whole relevant range of model parameters, the expansion velocity at R_* is still subsonic (except for the hottest and densest models, cf. Sect. 4.3.3). Thus, R_* can be regarded as the radius of the hydrostatic stellar core.

The "stellar temperature" T_* is defined by the luminosity L and the stellar radius R_* via the Stefan-Boltzmann law, i.e. T_* denotes the effective temperature referring to the radius R_*.

Table 1. Model atom summary

Ion	No. of levels	No. of lines
He I	17	55
He II	16	120
He III	1	0
N II	1	0
N III	33	118
N IV	38	153
N V	17	80
N VI	1	0
Total	124	526

The problem of defining a reference radius and, correspondingly, of any "effective temperature" in spherically extended atmospheres has been addressed in previous papers (e.g. Hamann 1994).

Only Doppler broadening is accounted for in the profile function of the line absorption coefficient. The Doppler-velocity $v_{\rm D}$ reflects random motion on small scales and is generally set to $100\,{\rm km\,s^{-1}}$. A "microturbulence" of that order-of-magnitude reproduces best the detailed shape of the observed line profiles. Its precise value does not have significant influence on the results of our spectral analyses.

The line radiation transfer in the spherically expanding geometry is formulated in the comoving-frame of reference (CMF), treating correctly the overlap of blending lines. Continuum formation is treated with the moment equations and variable Eddington factors.

The equations of statistical equilibrium account for all relevant radiative and collisional transition rates. The temperature stratification is calculated from the assumption of radiative equilibrium. The consistent solution of both sets of equations, radiation transfer and statistical equilibrium, is achieved by "iteration with approximate lambda operators", taking advantage of "Broyden's method" in the solution algorithm (Koesterke et al. 1992).

The obtained non-LTE population numbers enter the subsequent Formal Integration of the transfer equation in the observer's frame which is performed by straightforward integration along each ray. Frequency redistribution of line photons by electron scattering is accounted for in that stage.

The model atmosphere is assumed to consist of helium and nitrogen. The model atoms are nearly the same as described in Hamann et al. (1994). Their complexity is summarized in Table 1. Low-temperature dielectronic recombination is taken into account for N III and N IV.

Adopting the described "standard model" assumptions, any particular WR atmosphere is specified by its chemical composition and the basic parameters T_*, R_*, $\dot{M}$, v_∞.

3. Grids of models, and the subtype domains

For a given fixed chemical composition and a given stellar temperature T_*, synthetic spectra from Wolf-Rayet model atmospheres of different mass-loss rates, stellar radii and terminal

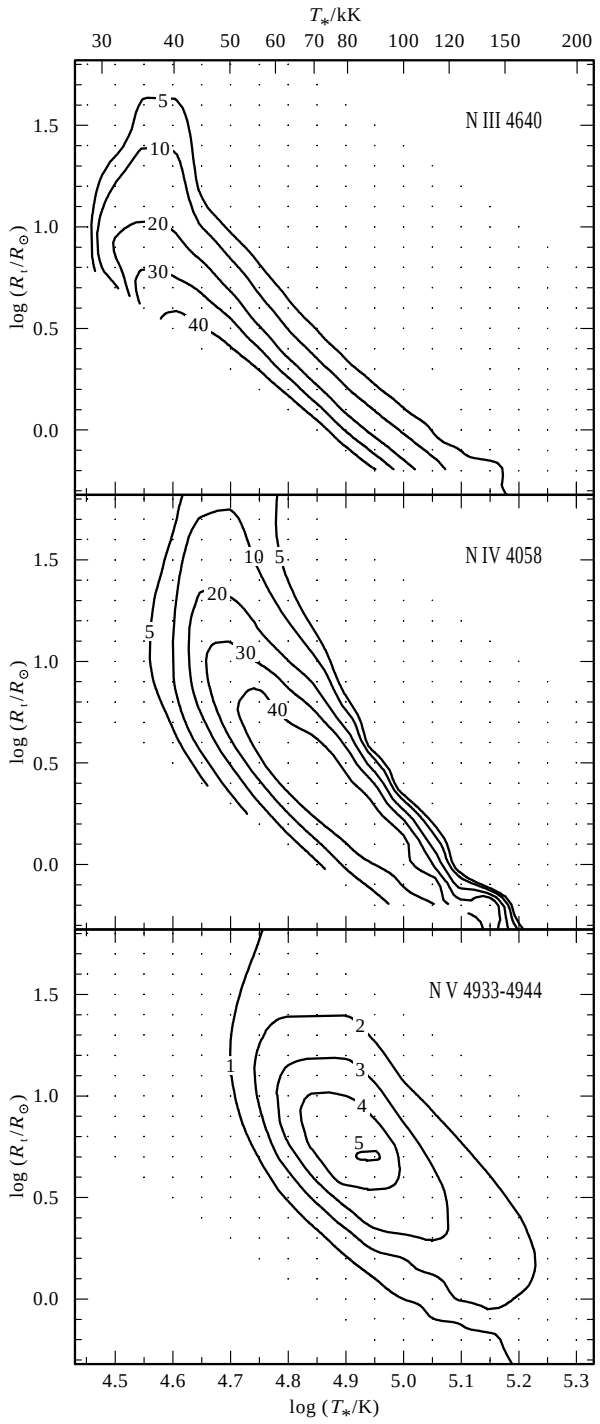

Fig. 1. Contours of constant line emission, labelled with the equivalent width in Å, for WN classification lines of nitrogen. Tiny dots indicate the calculated grid models (v_∞ = 1600 km/s).

wind velocities yield almost the same emission line equivalent widths, if they agree in their "transformed radius" R_t defined by

$$R_\mathrm{t} = R_* \left[\frac{v_\infty}{2500\,\mathrm{km\,s^{-1}}} \Big/ \frac{\dot{M}}{10^{-4}\,M_\odot\,\mathrm{yr}^{-1}} \right]^{2/3} . \qquad (1)$$

Note that R_t is inversely correlated with the mass-loss rate, i.e. the smaller the transformed radius the higher is the density in the stellar wind.

This scaling law was discovered by Schmutz et al. (1989) and validated by various numerical experiments with reasonable accuracy. (From the theoretical viewpoint this is rather surprising, as the scaling law implies that only those processes in the stellar atmosphere are relevant which scale with the square of the density.) For a given v_∞ even the spectra (continuum shape and line profiles) are invariant if R_t is kept constant, apart from a scaling of the absolute fluxes with R_*^2.

Thus, for a grid of models only two parameters (T_*, R_t) must be varied if the terminal wind velocity is set to a fixed value. We calculate two model grids, one with v_∞ = 1600 km/s as typical for late and medium WN subtypes, and another with 2500 km/s which is more adequate for the earliest subtypes. For the nitrogen abundance we adopt a mass fraction of 1.5% as an approved value for fitting the Galactic WN spectra (e.g. Hamann et al. 1994).

As an initial guess for the average luminosity, we calculate the model grids for $\log L/L_\odot = 5.3$. Stefan-Boltzmann's law than implies the stellar radius for any given T_*.

About 300 models were calculated in each of the two grids. T_* is varied between 28.2 kK ($10^{4.45}$ K) and 200 kK ($10^{5.30}$ K) in steps of 0.05 dex, while R_t ranges from 0.4 $R_\odot$ ($10^{-0.4}$ $R_\odot$) to 100 $R_\odot$ in steps of 0.1 dex. The tiny dots in Figs. 1 and 3 indicate the calculated models. The detailed emergent spectrum is calculated for each model, ready for comparison with any observed data (cf. Sect. 4).

For a general orientation in the parameter space we recalculate the Formal Integral for the classification lines, now suppressing any neighboring blends, and evaluate the equivalent widths. Frequency redistribution by electron scattering is also suppressed for that purpose, because (i) it is unclear to what extend electron scattering line wings are included in measured equivalent widths, and (ii) these wings will be drastically reduced in future models which account for "clumping". The results are presented in Fig. 1 in the form of contour plots. (The shown contours refer to the grid with v_∞ = 1600 km/s, but the corresponding diagrams for the grid with v_∞ = 2500 km/s are almost identical.) As to be expected, N III (considered line at 4640 Å) is strongest at low temperatures and small transformed radii (i.e. high density). N IV (classification line at 4058 Å) has its maximum strength at intermediate temperatures, the strip being inclined because higher temperatures are required to compensate the increase of the recombination rates at higher density. N V (considering the multiplet at 4603-4619 Å) occurs between 60 and 150 kK, reaching maximum strength around T_* = 90 kK.

These model predictions can be compared with the criteria defined for the subtype classification of WN stars. Following Smith (1968), the subtypes WN5 and WN6 are characterized by a similar line strength of N III and N IV. Allowing a factor of four between the equivalent widths of the corresponding classification lines, this criterion is fulfilled in the shaded strip indicated in Fig. 2. To the cooler side of that strip we have N III $\gg$ N IV, i.e. the WNL domain. Vice versa, WNE stars of subtype

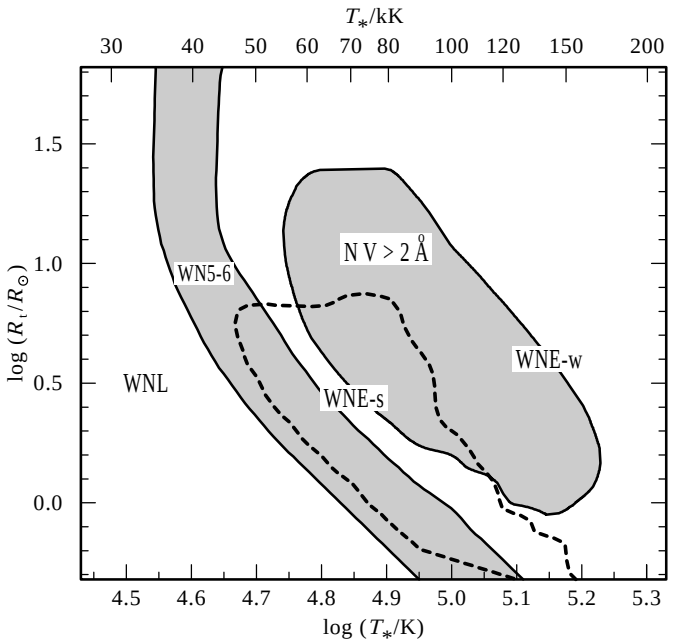

Fig. 2. Subtype domains, as obtained when the classification criteria of Smith (1968) are applied to the grid of models. Within the WN5-6 strip (shaded), the emission equivalent widths of the N III line at 4640 Å and the N IV multiplet at 4058 Å are roughly equal (within a factor of four). To the cooler side from that strip, the N III line is much stronger than N IV (WNL domain), while on the hotter side N III is much weaker than N IV (i.e. subtypes earlier than WN5). The N V lines are strong in the closed shaded region (shown: N V 4933-4944 stronger than 2 Å). The dashed contour encloses the region in which He II 5412 is stronger than 37 Å, leading to the classification as WNE-s.

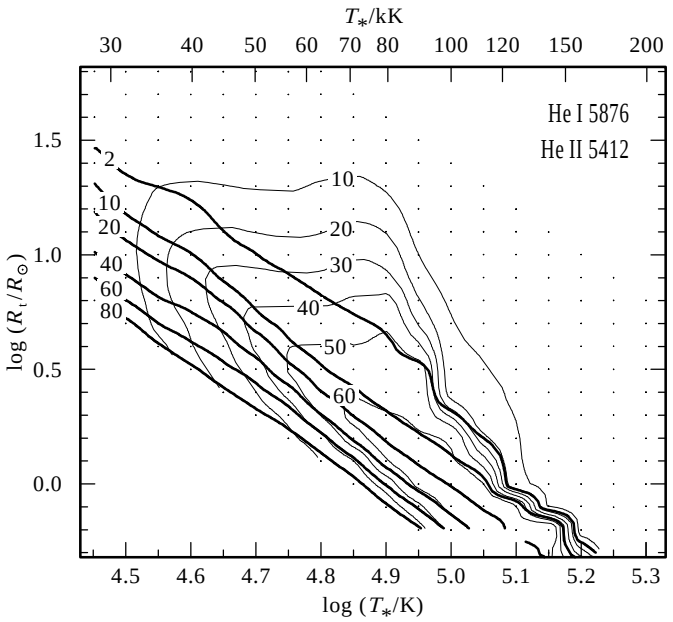

Fig. 3. Contours of constant line emission, labelled with the equivalent width in Å, for strategic helium lines (thick contours: He I, thin: He II). Tiny dots indicate the calculated grid models (v_∞ = 1600 km/s).

WN4.5 and earlier are resided on the hotter side of the WN5-6 strip. As these stars show N V lines by definition, they must be located inside the shaded region enclosed by the 2 Å contour of N V 4933-44. Moreover, WNE stars are divided into the strong-lined (WNE-s) and the weak-lined (WNE-w) subgroup, depending on the equivalent width of He II 5412. The WNE-s domain is encircled by a dashed curve in Fig. 2. Thus, the detailed analysis of any WN spectrum should yield parameters which are consistent with the appropriate subtype domain.

Contour plots of the strategic helium lines He I 5876 and He II 5412 are shown in Fig. 3. These lines have been used for our previous pure-helium analyses (Schmutz et al. 1989, Paper I). Their new contours do not differ much from the old ones (Schmutz et al. 1989), although the latter were calculated with much simpler models (pure helium composition, "grey" temperature structure). However, the present grid extends to higher temperatures than our former calculations which terminated at 90 kK. Note that a specific He I contour which intersects a specific He II contour at low temperatures (take, for instance both 20 Å contours intersecting at 38 kK), may come close to each other a second time at high temperatures above 100 kK. The possibility of a "second solution" for the helium fit will be discussed below (Sect. 4.3.2).

4. The analyses

4.1. The Galactic WN stars: identification and classification

The mple of program stars (cf. Table 2) is identical with that of Paper II and comprises the vast majority of the known Galactic WN stars, excluding those stars which definitely show composite spectra because of a luminous companion. The stars are identified by their WR number referring to the Catalog by van der Hucht et al. (1981). The spectral subtype classification (Table 2, Column 2) is also quoted from van der Hucht et al. (1988) in general. The WN subtype number essentially reflects the line strength ratios between different ionization stages of nitrogen. Remember that the subtypes WN2 to WN6 are called "early" (WNE), while from WN7 they are termed "late" (WNL). An additional "a" (abbreviating "+abs") is attributed according to van der Hucht et al. (1988) to those spectra showing not only emission, but also "absorption lines which have not been shown to be due to a companion", i.e. that might be intrinsic. A "+c" added to the spectral type denotes putative single-lined spectroscopic binaries. For WNE stars we append "-w" or "-s" to the classification, indicating whether the emission lines are weak or strong, respectively. The criterion is whether the equivalent width of the He II line at 5412 Å is smaller or larger than 37 Å (cf. Paper II).

Smith et al. (1996) proposed a refined, three-dimensional classification scheme for WN stars. Their classification of our program stars is given in Table 2, Column 3. In our discussion we maintain the old classification, because it is based on nitrogen lines alone, while the new scheme involves helium lines as well. As we want to analyze the nitrogen spectra in the present paper, the former is more suitable for our purpose. Moreover, our criterion for weak and strong lined WNE stars (see above) is

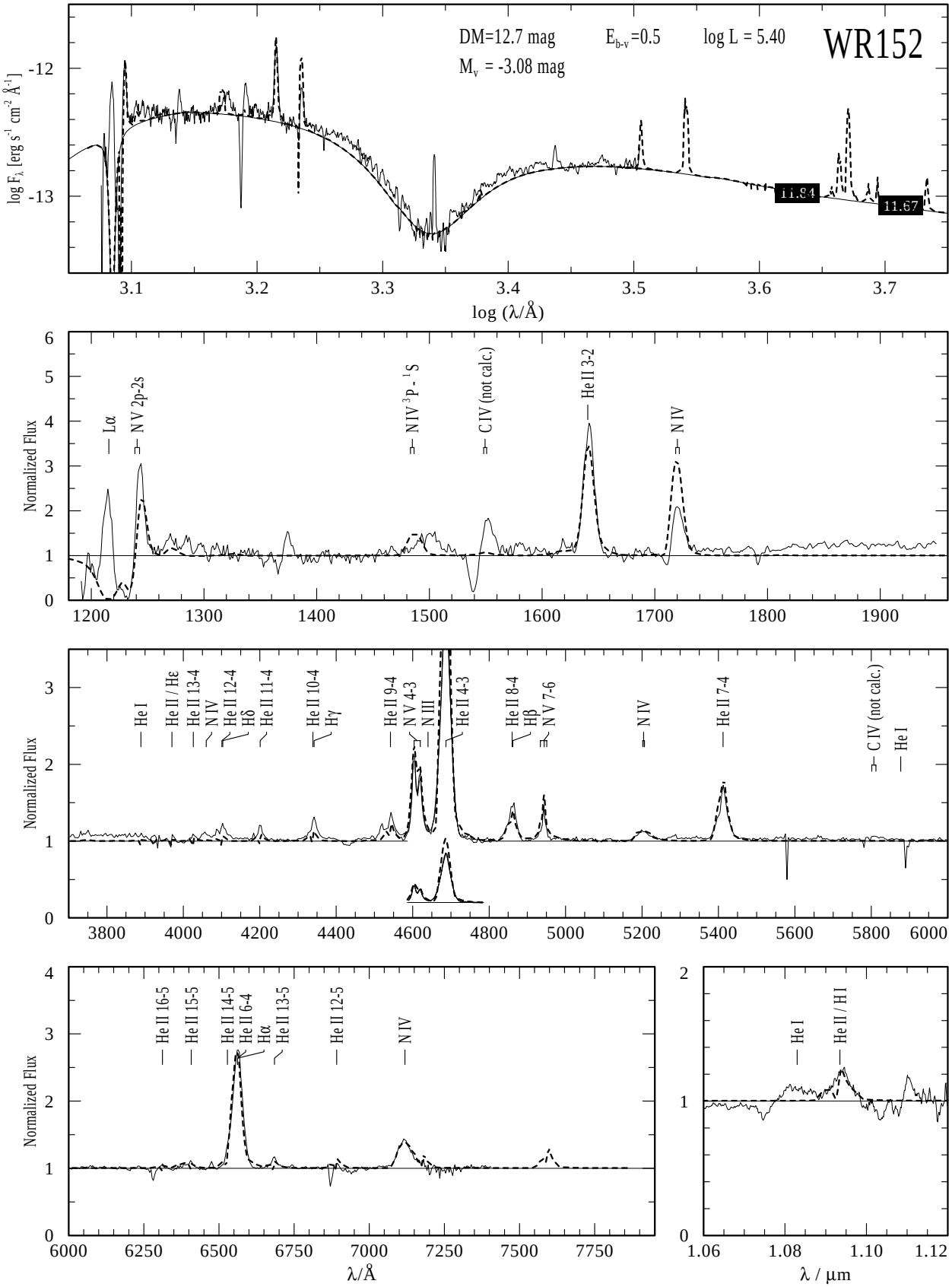

Fig. 4. Spectra of WR 152 plotted with the best-fitting model (T_* = 79.4 kK, R_t = 12.6 $R_\odot$) from the grid with v_∞ = 1600 km/s. The model flux is appropriately reddened and scaled in order to match the calibrated observation (IUE, m_b and m_v), implying the values for L and M_v as indicated in the figure.

easy to compare with the models (cf. the corresponding contour in Fig. 2), while the corresponding "b" criterion by Smith et al. (1996) involves more complicated quantities.

4.2. The observations

The observational material is the same as employed in Papers I and II and has been published in our atlas of WN spectra (see Hamann et al. 1995b for more details). These spectra were taken at the "Deutsch-Spanisches Astronomisches Zentrum (DSAZ)", Calar Alto, Spain, and at the European Southern Observatory (ESO), La Silla, Chile. Additionally, we have retrieved IUE low resolution spectra from the archive for all program stars if available. The IUE data were smoothed over 5 Å. Any theoretical spectra were degraded to the spectral resolution of the observation before plotting the comparison.

4.3. The spectral fits

In order to compare the observed spectra with the grid models, we created working plots for each of the program stars. An example (for WR 152, WN3-w) is shown in Fig. 4. The upper panel gives absolute fluxes and contains the IUE observation together with the b and v narrow-band photometry (taken from the compilation by van der Hucht et al. 1988). The other panels display normalized spectra for the IUE-short UV, visual range and the 10830 Å region. (The set of data is not complete for all program stars.) The observed visual and IR spectra taken from our spectral atlas (Hamann et al. 1995b) were normalized to the continuum by fitting a low-order polynomial through continuum points chosen "by eye". The UV spectrum (second panel) is normalized by division by the theoretical continuum of the selected model (cf. Sect. 4.4).

Now we pick out a computed model from one of our two grids, taking that grid with the more appropriate terminal velocity for the considered star. The theoretical spectrum (dashed in Fig. 4) is plotted together with the observation. Using this type of diagram we compared each of the program stars with several grid models in order to select the best-fitting model.

Generally, convincing fits are obtained. Column 16 of Table 2 gives a rating of the achieved fit quality. The example shown in Fig. 4 is a "very good" fit in our scale. The uncertainty in the selection of the final model is plus or minus one grid mesh in temperature and transformed radius, typically. However, we encounter also notorious discrepancies between models and observations, which are discussed in the following.

4.3.1. WNL subtypes

For WNL stars, we generally derived similar parameters as we had obtained from the pure-helium analyses in Papers I and II. This is in line with the results of Crowther (1994, 1995a,b) who had re-analyzed some ten Galactic WNL stars by means of models with nitrogen, and also confirmed the previously estimated parameters.

4.3.2. WNE-w subtypes

Quite different experiences are made with WNE-w stars. One example fit is shown in Fig. 4. The nitrogen spectrum of WR 152 (WN3-w) is nicely reproduced by a model with T_* = 79.4 kK, while the pure-helium analysis yields only 35.5 kK (Paper I). Our new result is corroborated by Crowther et al. (1995c) who obtained 69 kK for that star from a fine analysis including nitrogen.

The origin of this discrepancy between helium and nitrogen analysis is closer illustrated in Fig. 5. Taking the (WN4-w) star WR 44 now as example, a section from the visual spectrum is displayed and compared to different models in the three panels. In the top panel (a) the selected model fits the helium lines (parameters as of Paper II, roughly). While the He II lines (4686 Å, 5412 Å) are matched well, the He I line at 5876 Å is reproduced in its strength, but not in the detailed profile shape (note that this line is affected by the neighboring C IV blend which is not accounted for in the model, and depressed by the unresolved Na I interstellar absorption doublet). However, this model fails completely to fit the nitrogen lines. It predicts strong N III 4640, while the observed feature is obviously due to N V 4603,4619. N V 4933-4944 is also observed but not visible in the synthetic spectrum.

At a much higher stellar temperature (T_* = 70.8 kK, $R_{\rm t}$ = 10.0 $R_\odot$) the model reproduces the nitrogen spectrum almost perfectly (Fig. 5b). This model shows the N V lines in the observed strength, while N III has vanished. The N V line at 5202-5206 Å is a bit stronger than observed, while other N IV features (1720 Å, 4058 Å, 7119 Å – not shown in Fig. 5) are in even better agreement. Thus, the nitrogen fit enforces us to adopt the stellar parameters as employed in Fig. 5b. However, this model does not show any He I 5876 line, contrary to the observation.

There is no parameter combination in our grid which resolves this discrepancy. The He I lines require a lower temperature and/or a smaller $R_{\rm t}$ in order to reach the observed strength. Fig. 5c demonstrates that a model with the same temperature (70.8 kK) as in panel b) reproduces the He I 5876 line perfectly (even in its profile shape), if the transformed radius is as small as 3.98 $R_\odot$. I.e., compared with the model in b) the density (mass-loss rate) is higher by a factor of four. All other lines (He II, nitrogen) are much too strong in that model, including their electron-scattering wings.

Thus, in terms of the contour diagrams from Sect. 3, there is not really a "second solution" for the helium lines at higher temperatures. However, from the nitrogen calculations those high temperatured are mandatory for WNE stars in order to produce the observed N V. Vice versa, the discrepancy with He I at the hot "nitrogen solution" is not so severe, as the matching He I contour passes in the vicinity, at somewhat higher density.

Even within the nitrogen spectra inconsistencies of that kind are encountered. Observed WN5 and WN6 spectra per definition show N III, N IV and N V lines simultaneously, for WN5 even with similar strength for these three ions. However, the contour plots in Fig. 1 reveal that, according to our models, the WN5-6 strip and the N V domain do not overlap. Consequently, those

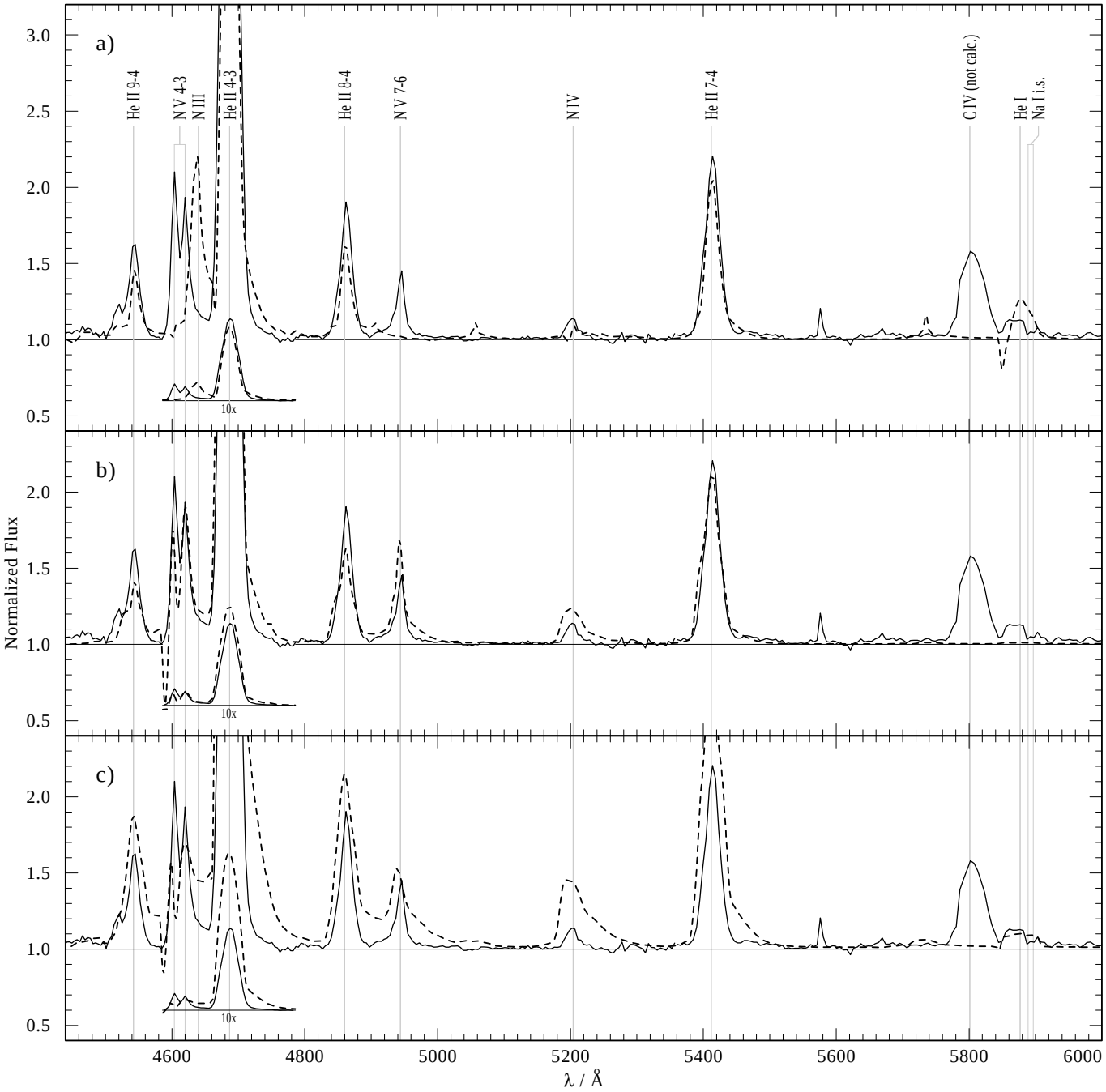

Fig. 5. Part of the observed spectrum of WR 44 (WN4-w; thin line), compared with three different models (dashed) demonstrating the inconsistency between the helium and nitrogen line analysis. **a)** Grid model which reproduces best He II 5412 and He I 5876 (T_* = 39.8 kK, R_t = 12.6 $R_\odot$). This model predicts strong N III 4640, while the observed feature is obviously due to N V 4603,4619. **b)** Grid model which reproduces best the nitrogen lines (T_* = 70.8 kK, R_t = 10.0 $R_\odot$). This model also fits the He II lines, but fails completely to reproduce He I 5876. **c)** Model with same stellar temperature as in panel b), but higher wind density (R_t = 3.98 $R_\odot$). This model reproduces He I 5876 perfectly, but is in contradiction to all other lines. See text for further discussion

spectra showing both N III and N V are not fitted consistently by one unique model. The same problem was already described in the detailed study of WR 136 by Hamann et al. (1994).

At the moment we do not know how to resolve this discrepancy. Models with metal line blanketing are under construction presently by Hillier and coworkers (cf. Hillier 1990) and by our group. As far as first results show (Hillier and Miller 1998), the inclusion of blanketing has significant impact on some of the nitrogen lines. Even our neglection of carbon as a cooling agent might affect a few sensitive features (e.g. N IV 1486). However, we suggest that *clumping* is the major cause for the described problems. Evidence for wind inhomogeneities come from the

electron scattering wings of strong lines, which are predicted too strong by the homogeneous models (as marginally visible in Figs. 4 and 5). The densest parts of these clumps, possibly filling only a small volume fraction, would contain the material with the lowest ionization stages, producing preferably the He I and N III emission, while highest ions are present in the diluted, inter-clump medium. Thus we think that fitting mainly the lines of the leading ions gives a reasonable approach to reality, as long as we are restricted to homogeneous models (see also Sect. 6). For the analyses in this paper we disregard any discrepancies with He I lines and only aim at nitrogen. For spectra showing N III and N V lines simultaneously we seek a compromise fit. For these (WN5 and WN6) subtypes the internal uncertainty of the fit parameters is largest (plus or minus two grid cells in T_* and $R_{\rm t}$, typically).

The decision for the "nitrogen solution" has dramatic effects on the derived parameters for the WNE-w stars. According to the helium fits performed in Papers I and II, the WNE-w stars were thought to be as "cool" as the WNL with temperatures around 40 kK. The nitrogen fits now require much hotter temperatures which imply considerably higher luminosities (see Sect. 5.2) for that spectral subgroup.

4.3.3. The WN stars of earliest subtype

In the spectra of three program star (WR 2, WR 3, WR 46) no He I lines are detectable. Hence it was not possible to analyze these stars with the technique of Papers I and II. But, due to the progress in the model calculations, we can now analyze these stars now using their nitrogen lines. This has been done for WR 46 by Crowther et al. (1995c), while corresponding results for WR 2 and WR 3 are presented here for the first time. With a stellar temperature T_* of about 140 kK, WR 2 is the hottest known Galactic WN star.

For the hottest and densest models of our grid, just as appropriate for WR 2, the wind velocity at Rosseland optical depth $\tau_{\rm Ross} = 20$ (i.e. per definition at R_*, the standard location of the lower boundary of our model atmosphere) is not small (i.e. not sub-sonic). In order to test for a possible over-estimate of the hydrostatic core radius we performed additional calculations extending to $\tau_{\rm Ross} = 100$ and obtained no significant differences.

4.3.4. WNE-s subtypes

The problems with modelling the lines from low ions (He I, N III) simultaneously with N V and N IV described above for WNE-w stars appear also in early subtypes with strong lines. However, for these stars the impact on the derived parameters is only small, for the following reason. In the WNE-s spectra the He II lines are close to their maximum strength, i.e. the helium solution lies close to the top of the "mountain" formed by the He II 5412 contours shown in Fig. 3. Thus, if the nitrogen fit enforces us now to take the solution at the hot flank of that mountain instead of the cool side, this does not make a big difference. Consequently, the nitrogen fit does not lead to much higher temperatures and luminosities for WNE-s stars, contrary to the experience with WNE-w stars described above.

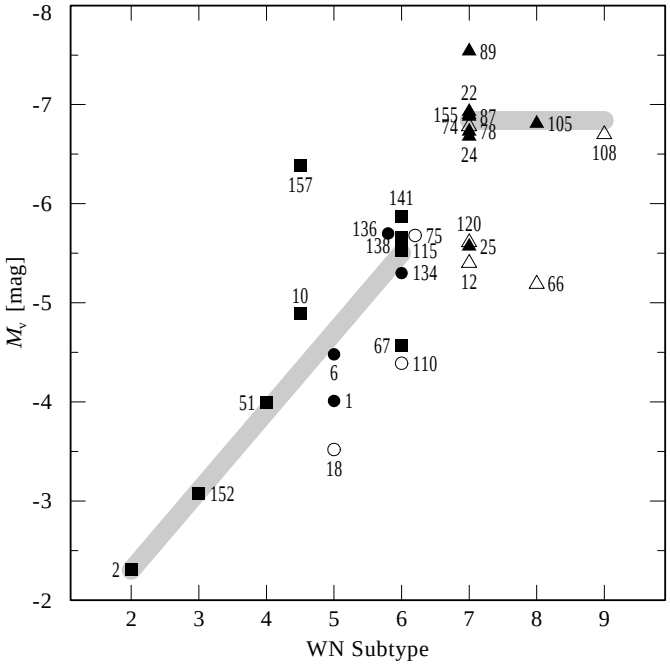

Fig. 6. Absolute visual magnitudes of WN stars with distances being known from cluster or association membership (definite or probable membership: filled symbols; possible membership: open symbols) versus spectral subtype. The stars are identified by their WR number, and symbol shapes refer to the spectral subgroups (cf. Fig. 7). We adopt the shaded relations for the calibration of those WN stars with unknown distance.

4.4. Absolute fluxes

For fitting the absolute flux (top panel in Fig. 4), two more parameters can be adjusted, the luminosity L and the color excess E_{b-v}. The former acts as a scaling factor of the model flux (remember that the grid models were calculated for $\log L/L_\odot$ = 5.3), while the latter is applied for the interstellar reddening using the law of Seaton (1979) augmented by interstellar Lα absorption. The use of a standard law is inevitable for a comprehensive study, although it might be questioned for individual stars. Crowther et al. (1995b) found anomalous reddening towards WR 25. Testing the alternative reddening law by Cardelli et al. (1988) which implies stronger absorption below 1500 Å, we obtain worse fits in most cases, but also better agreement for few stars.

The values for E_{b-v} are taken from the previous papers as a first guess, but are properly adjusted if necessary. The final values are given in Table 2, Column 8, and marked with an asterisk if they were improved with respect to Paper II. Due to the inclusion of the IUE data and the application of the nitrogen model continua, the new values are certainly more reliable. Typical corrections of E_{b-v} are of the order of 0.1 mag, with a systematic tendency to increased reddening compared to Paper II. For

Table 2. Parameters of the Galactic single WN stars

WR	Spectral subtype†		T_*	R_t	v_∞	β_H	E_{b-v}	DM	M_v	R_*	$\log \dot{M}$	$\log L$	$\frac{\dot{M} v_\infty}{L/c}$	M	Q‡
	Smith 68	SSM 96	[kK]	$[R_\odot]$	[km/s]	[%]	[mag]	[mag]	[mag]	$[R_\odot]$	$[M_\odot$/yr]	$[L_\odot]$		$[M_\odot]$	
(1)	(2)	(3)	(4)	(5)	(6)	(7)	(8)	(9)	(10)	(11)	(12)	(13)	(14)	(15)	(16)
1	WN5-s	WN4b	100.0	1.58	2000	0	0.59	12.1	→ -4.01	1.5	-4.1	5.3	36.3	13	3
2	WN2-w	WN2b	141.3	1.26	3100	0	0.49*	12.0	→ -2.31	0.5	-4.5	5.0	51.6	9	4
3	WN3a-w +c	WN3b+O4	89.1	12.59	2500	0	0.33	12.5	← -3.10	2.5	-5.1	5.6	3.1	18	2
6	WN5-s +c?	WN4b	100.0	1.58	1700	0	0.03	11.3	→ -4.48	1.8	-4.1	5.4	24.0	16	2
7	WN4-s	WN4b	89.1	2.51	1600	0	0.46	13.8	← -3.90	1.9	-4.4	5.3	16.4	13	3
10	WN4.5-w	WN5h(+OB)	63.1	25.12	1500	25	0.60*	13.3	→ -4.89	7.5	-5.0	5.9	0.9	28	3
12	WN7 +c	WN8h	35.5	6.31	1100	27	0.65*	15.2	← -6.84	19.9	-3.6	5.8	23.7	23	2
16	WN8	WN8h	31.6	10.00	900	20	0.50*	13.2	← -6.84	25.1	-3.8	5.8	11.3	23	2
18	WN5-s	WN4b	100.0	2.00	2100	0	0.64	13.3	← -4.70	2.4	-4.0	5.7	22.3	22	2
20	WN4.5-w	WN5o	50.1	10.00	1400	0	1.05*	14.6	← -4.30	5.9	-4.6	5.3	8.9	13	4
22	WN7a +c	WN7ha	35.5	25.12	1000	40	0.31*	12.1	→ -6.93	26.5	-4.4	6.0	2.1	33	5
24	WN7a	WN6ha	35.5	31.62	1200	44	0.26	12.1	→ -6.68	23.6	-4.5	5.9	2.3	28	2
25	WN7a	WN6ha	35.5	31.62	1200	53	0.40*	12.1	→ -5.57	13.3	-4.9	5.4	3.1	15	5
28	WN7	WN6(h)	– no observation –												
29	WN7	WN7h+abs	– no observation –												
34	WN4.5-w	WN5o	63.1	6.31	1200	0	0.97	14.8	← -4.30	4.5	-4.5	5.4	6.0	16	4
35	WN6-w	WN6h	39.8	10.00	1100	22	1.01	15.2	← -5.50	11.2	-4.3	5.4	10.0	16	2
36	WN4-s	WN5-6b	89.1	2.51	2100	0	0.95*	13.6	← -3.90	2.0	-4.2	5.3	27.4	14	3
37	WN3-s	WN4b	79.4	3.98	2150	0	1.70*	12.1	← -3.10	1.9	-4.6	5.1	23.5	10	2
40	WN8	WN8h	31.6	7.94	1000	15	0.30*	13.5	← -6.84	23.7	-3.7	5.7	20.3	22	2
44	WN4-w	WN4o	70.8	10.00	1400	0	0.61	14.4	← -3.90	4.0	-4.9	5.6	2.7	18	3
46	WN3pec-w	WN3b pec	89.1	7.94	2300	0	0.27	13.0	← -3.10	2.2	-4.9	5.4	5.5	16	1
49	WN5-w	WN5(h)	70.8	10.00	1450	25	0.90*	14.5	← -4.30	4.7	-4.7	5.7	2.7	22	3
51	WN4-w	WN4o	63.1	10.00	1300	0	1.45*	12.8	→ -3.99	4.7	-4.8	5.5	3.4	17	2
54	WN4-w	WN5o	70.8	7.94	1300	0	0.80*	13.6	← -3.90	3.7	-4.8	5.5	3.4	17	2
55	WN7	WN7o	39.8	7.94	1100	0	0.63	15.1	← -6.84	19.9	-3.8	5.9	10.6	30	5
58	WN4-s	WN4b/CE	79.4	3.16	1600	0	0.63*	14.4	← -3.80	2.4	-4.4	5.3	16.4	13	2
61	WN4.5-w	WN5o	44.7	10.00	1400	0	0.65*	14.2	← -4.30	6.3	-4.6	5.2	13.6	11	3
62	WN6-s	WN6b	44.7	5.01	1800	0	1.90*	11.9	← -5.50	8.9	-3.8	5.4	53.5	16	5
63	WN6	WN7o+OB	– no observation –												
66	WN8	WN8(h)	31.6	10.00	1500	5	1.00	14.5	← -6.84	25.1	-3.6	5.8	31.4	23	2
67	WN6-w	WN6o	39.8	10.00	1500	0	0.97	12.8	→ -4.57	7.5	-4.4	5.1	22.8	10	5
71	WN6 +c	WN6o	– no observation –			0									
74	WN7	WN7o	39.8	7.94	1300	0	1.90*	13.0	→ -6.78	18.8	-3.7	5.9	15.3	28	4
75	WN6-s	WN6b	56.2	5.01	2300	0	1.00*	13.0	→ -5.68	8.4	-3.7	5.8	35.9	25	5
78	WN7	WN7h	35.5	9.95	1200	15	0.45	11.5	→ -6.73	22.3	-4.2	5.8	4.7	27	2
82	WN8	WN7(h)	39.8	7.94	1100	20	1.07	14.9	← -6.84	19.9	-3.8	5.9	10.6	31	4
83	WN6	WN5o	– no observation –												
84	WN6-w	WN7o	39.8	10.0	1100	0	1.50	12.9	← -5.50	11.9	-4.2	5.5	9.7	17	5
85	WN6	WN6h	– no observation –			+									
87	WN7	WN7h+abs	35.5	25.12	1400	40	1.75*	12.3	→ -6.88	26.5	-4.2	6.0	4.2	33	5
89	WN7	WN8h+abs	35.5	31.62	1600	20	1.65*	12.3	→ -7.54	35.4	-4.1	6.3	3.4	47	3
91	WN6-s	WN7b	44.7	3.98	1700	0	1.80*	14.3	← -5.50	7.9	-3.7	5.3	71.3	14	2
94	WN6	WN5o	– no observation –												
100	WN6-s	WN7b	44.6	3.98	1600	0	1.40	13.2	← -5.50	7.9	-3.7	5.3	63.6	14	2
105	WN8	WN9h	31.6	15.84	700	17	2.13	11.0	→ -6.81	26.6	-4.2	5.8	3.3	25	2
107	WN7-8	WN8o	– no observation –												
108	WN9	WN9ha	31.6	31.62	900	27	1.01	12.7	← -6.70	26.6	-4.6	5.8	2.0	25	2
109	WN3	WN5h	– no observation –												
110	WN6-s	WN5-6b	89.1	2.51	2300	0	0.90*	12.1	← -5.50	4.0	-3.7	5.9	23.3	30	5

(to be continued)

Table 2. (continued)

WR	Spectral subtype†		T_*	R_t	v_∞	β_H	E_{b-v}	DM		M_v	R_*	$\log \dot{M}$	$\log L$	$\frac{\dot{M}v_\infty}{L/c}$	M	Q‡
	Smith 68	SSM 96	[kK]	$[R_\odot]$	[km/s]	[%]	[mag]	[mag]		[mag]	$[R_\odot]$	$[M_\odot$/yr]	$[L_\odot]$		$[M_\odot]$	
(1)	(2)	(3)	(4)	(5)	(6)	(7)	(8)	(9)		(10)	(11)	(12)	(13)	(14)	(15)	(16)
115	WN6-w	WN6o	39.8	12.59	1280	0	1.50*	11.7	→	-5.53	12.6	-4.3	5.6	9.1	18	2
116	WN8	WN8h	31.6	7.94	800	10	1.69	13.3	←	-6.84	25.1	-3.7	5.8	12.6	23	3
120	WN7	WN7o	35.5	10.00	1020	0	1.35*	13.6	←	-6.84	23.6	-3.8	5.9	9.4	28	2
123	WN8 +c	WN8o	31.6	7.94	1020	0	0.71	15.2	←	-6.84	23.7	-3.7	5.7	21.1	22	2
124	[WN8]? +c	WN8h	31.6	7.94	700	13	1.10	13.9	←	-6.84	25.1	-3.8	5.8	9.7	23	2
128	WN4-w +c	WN4(h)	63.1	19.95	1500	20	0.32*	13.1	←	-3.90	4.7	-5.2	5.5	1.6	17	2
129	WN4-w	WN4o	70.8	10.00	1320	0	0.95*	13.3	←	-3.90	4.2	-4.8	5.6	2.4	19	2
130	WN8	WN8(h)	31.6	15.84	1000	12	1.46	13.5	←	-6.84	26.6	-4.1	5.8	6.8	25	4
131	WN7a	WN7h+abs	35.5	31.62	1400	20	1.10*	14.7	←	-6.84	25.0	-4.4	5.9	3.1	30	2
134	WN6-s +c	WN6b	89.1	3.16	1900	0	0.47*	11.6	→	-5.30	4.2	-3.9	6.0	10.9	33	2
136	WN6-s +c	WN6b(h)	70.8	5.01	1600	12	0.50*	11.3	→	-5.70	7.5	-3.9	6.1	7.3	38	4
138	WN6a-w +c	WN5o+B?	39.8	19.95	1500	5	0.60*	11.3	→	-5.66	14.9	-4.4	5.7	5.7	22	3
141	WN6-w +c	WN5o+OB	39.8	10.00	1720	0	1.15*	11.3	→	-5.87	14.1	-3.9	5.7	21.9	20	3
147	WN7 +c	WN8(h)	35.5	19.95	1000	5	2.50*	11.5	←	-6.84	25.0	-4.3	5.9	3.1	30	3
148	WN7 +c	WN8h	35.5	31.62	1000	15	0.90*	13.6	←	-6.84	26.5	-4.5	6.0	1.5	33	3
149	WN6-s	WN5o	50.1	6.31	1100	0	1.50*	14.1	←	-5.50	9.4	-4.1	5.7	8.7	22	5
152	WN3-w	WN3(h)	79.4	12.59	1800	16	0.50*	12.7	→	-3.08	2.7	-5.2	5.4	2.5	15	1
155	WN7 +c	WN6o+09II/Ib	35.5	25.12	1300	0	0.65*	12.7	→	-6.90	25.0	-4.3	5.9	3.7	30	2
156	WN8	WN8h	31.6	12.59	700	30	1.20*	13.0	←	-6.84	26.6	-4.1	5.8	4.7	25	2
157	WN4.5-w	WN5o(+B1 II)	39.8	25.12	1500	15	0.85*	12.8	→	-6.38	19.9	-4.4	5.9	3.5	30	3
158	WN7	WN7h	35.5	25.12	900	30	1.05	14.0	←	-6.84	23.6	-4.3	5.9	1.8	28	3

* E_{b-v} values marked with an asterisk are modified with respect to Papers I and II

† Column 2: classification scheme of Smith (1968); Column 3: classification by Smith et al. (1996)

‡ Column 16: fit quality, ranging from 1 (very good) over 3 (satisfactory) to 5 (lousy); the systematic discrepancies with He I in WNE-w spectra (see Sect. 4.3.2) are disregarded in this rating

a couple of program stars this improvement of the reddening correction has significant impact on the derived luminosity.

The calculation of the predicted flux finally requires knowledge of the distance. Fortunately, many of our program stars can be assigned to an open cluster or association (Lundström & Stenholm 1984). We adopt the corresponding distance modulus in these cases (Table 2, Column 9). The absolute visual magnitude (Column 10) then follows.

These stars with known distance are used to "calibrate" the other program stars. Fig. 6 displays absolute visual magnitudes M_v versus the WN subtype numbers (Smith 1968 classification). As there is a nice correlation (shaded lines: linear between -2.3 mag (WN2) and -5.5 mag (WN6), and -6.84 as a average value for WNL) we adopt this for calibrating the M_v of the other program stars with unknown distance. Among the stars with "possible" cluster/association membership (open symbols in Fig. 6), WR 12, WR 18, WR 66 and WR 110 do not fit well into the relation. Therefore we decide to treat them like stars with unknown distance, although this conclusion is not stringent.

Consistent distance moduli DM and absolute visual magnitudes M_v for the program stars are given in Table 2, Columns 9 and 10. The arrows between these two columns indicate the flow of information, depending on whether DM is adopted and M_v follows, or vice versa.

The reddened and scaled model continuum is plotted in the top panel of our fit diagrams (Fig. 4) together with the flux-calibrated observation. In the second panel of Fig. 4 that theoretical continuum is used for automatic rectification of the observed IUE spectrum. If reddening and luminosity are adequately chosen, the UV observation is nicely rectified by the model continuum in most cases.

5. Results

5.1. Temperature and transformed radius

The parameters T_* and R_t of the best-fitting models are compiled in Table 2, Columns 4 and 5. In Column 6 we repeat, for easier reference, the terminal wind velocity v_∞ and the hydrogen mass fractions β_H from Paper II. Note that these parameters follow from the spectroscopic analyses alone, not involving any assumptions on the distance or absolute magnitudes of the stars. The positions of the program stars in the $\log T_*$-$\log R_t$-plane are plotted in Fig. 7. Still the WNL stars are found between

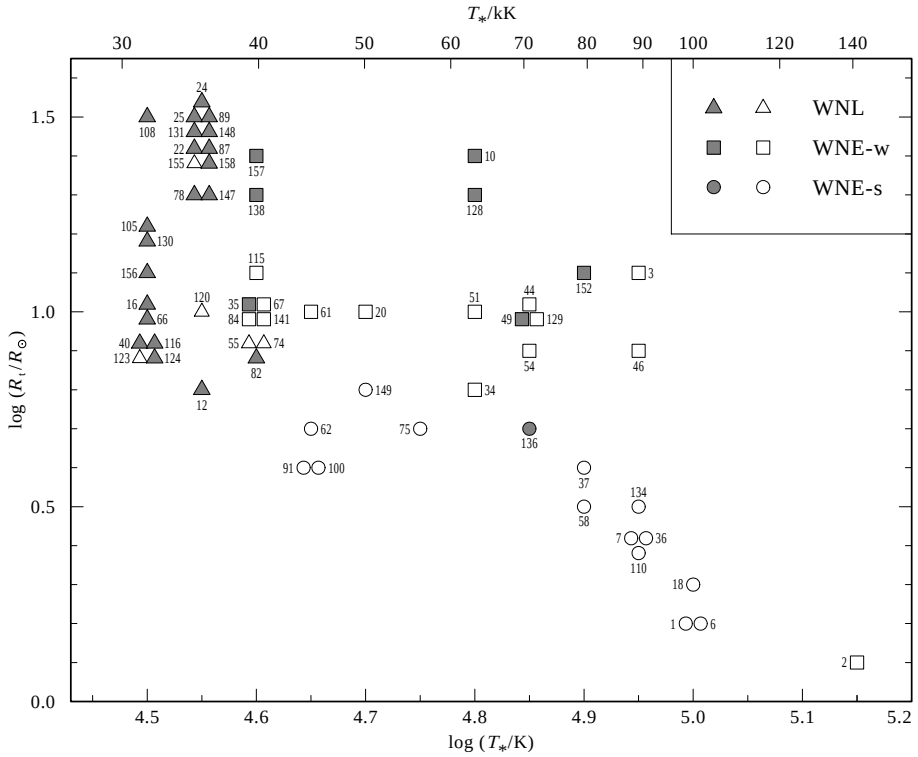

Fig. 7. Positions of the analyzed WN stars in the $\log T_*$-$\log R_t$-plane. The spectroscopic subclasses are distinguished by different symbol shapes (see inset). Filled symbols denote stars with hydrogen being detected in their spectra, while open symbols refer to stars without hydrogen.

30 and 35 kK, while the WNE-s stars populate a wide range of higher temperatures. Concerning the WNE-w stars, this diagram now differs remarkably from the previous versions in Papers I and II. These stars now scatter over the same range of high temperatures as the WNE-s stars, but the transformed radii are systematically larger, i.e. the weakness of the lines is due to lower wind densities.

The presence or absence of hydrogen is encoded in Fig. 7 by filled and open symbols, respectively. Hydrogen is generally found in WNL stars and absent in WNE-s subtypes. Concerning the WNE-w stars, those (seven out of 21) members of this group which show hydrogen have preferably higher transformed radii, i.e. weaker winds than the others.

5.2. Radius, luminosity and mass-loss rate

In Sect. 4.4 we have described how the luminosity is adjusted such that the – reddened and geometrically diluted – model flux matches the observed, absolutely calibrated flux or – for stars with unknown distance – reaches the absolute visual magnitude adopted for that star. The obtained $\log L$ values are compiled in Table 2, Column 13. Luminosity and stellar temperature imply the stellar radius R_* via Stefan-Boltzmann's law (Column 11). With R_t and v_∞ the transformation law (Eq. 1) yields the mass-loss rate (Column 12). We emphasize that radius, luminosity and mass-loss rate can be easily scaled to a different distance (or absolute magnitude) if desired.

From the stellar temperatures T_* and luminosities L an empirical Hertzsprung-Russell Diagram (HRD) can be constructed (Fig. 8). The meaning of the different symbols is the same as in Fig. 7.

The most striking difference against the previous version of that diagram (Schmutz et al. 1989, Papers I and II) arises from the revision of the WNE-w parameters. Due to the higher stellar temperatures, we now attribute much higher luminosities to the stars of this subclass (average $\log L/L_\odot$ = 5.5). Part of the WNE-s stars become slightly more luminous due to higher temperatures or larger reddening correction. Their average luminosity is the same as for the WNE-w stars ($\log L/L_\odot$ = 5.5). The WNL luminosities, not significantly revised, are highest ($\log L/L_\odot$ = 5.9).

Note that the luminosities given in Table 2 refer only to the emergent radiation. The stellar energy production must be higher, as part of the energy is consumed by the wind for its acceleration, for work against the gravitational potential and for the flow of enthalpy (Heger and Langer 1996). However, for our sample of WN stars this "wind darkening" is generally negligible: the average correction in luminosity amounts to 0.026 dex. Even for the WNE-s subtypes the wind adds only 0.06 dex to the luminosity, on the average. Exceptionally high is the wind luminosity of WR 2, increasing $\log L$ by 0.19 dex. We refrain from applying the wind darkening correction for the HRD, as we expect a downward revision of mass-loss rates by the inclusion of clumping in future models that will further reduce this effect.

The last column in Table 2 gives the current stellar mass, derived from the luminosity by means of the mass-luminosity relation for helium stars (Langer 1989). Note that this relation might not be adequate for those stars showing hydrogen. The average mass is 27 $M_\odot$ for WNL and 18 $M_\odot$ for WNE stars, respectively.

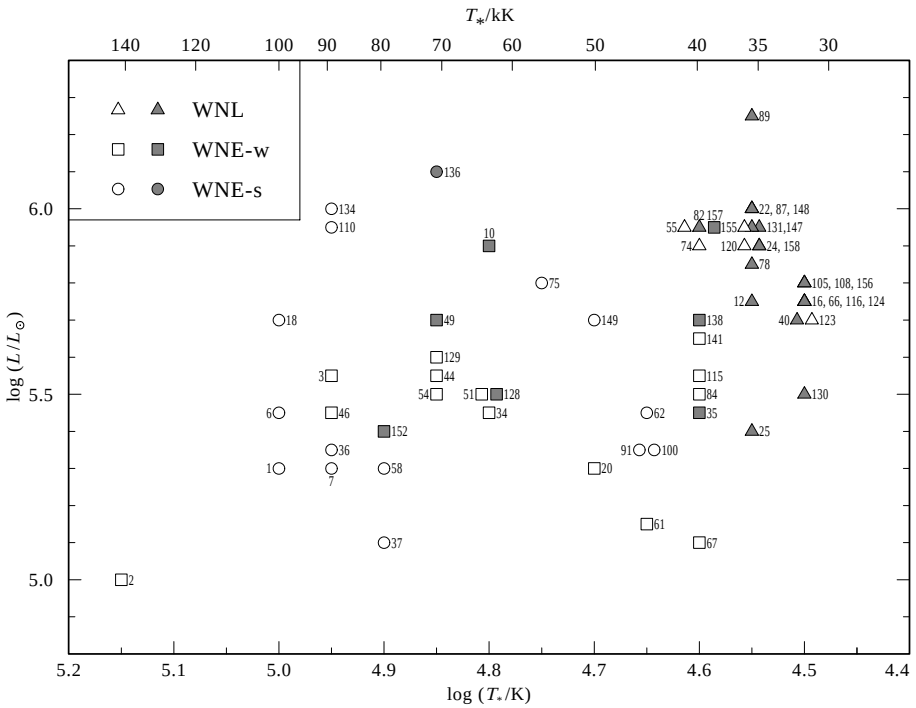

Fig. 8. Hertzsprung-Russell Diagram of the Galactic WN stars (labels: WR numbers). Different symbol shapes refer to the spectral subclasses (see inset). Full symbols represent stars with hydrogen in their atmosphere, while open symbols indicate that hydrogen is not detectable. The WNL stars concentrate at about 35 kK, while the WNE stars are hotter and scatter between 40 and 140 kK. In contrast to our previous results from the helium-line analyses, we now find that WNE-s and WNE-w stars populate the same region of the HRD. The luminosities range from $10^{5.0}$ to $10^{6.25} L_\odot$. Hydrogen is shown by the WNL and part of the WNE-w stars, with a few exceptions.

5.3. Mass-loss rate and momentum ratio

The mass-loss rates of the Galactic WN stars are given in Column 12 of Table 2. The average value for $\log\{\dot{M}/(M_\odot \mathrm{yr}^{-1})\}$ is -4.3, slightly higher than found in the previous papers.

The ratio between the mechanical momentum carried with the wind and the momentum of the radiation field, $\dot{M} v_\infty c/L$, is given in Column 14 of Table 2. Due to the revision of the WNE parameters, this ratio is now a bit lower than found in Papers I and II. But these numbers still exceed the "single-scattering limit" (i.e. unity) by far. The arithmetic averages are now 9, 9 and 29 for the WNL, WNE-w and WNE-s subclass, respectively. Among the WNE-w group the momentum ratio is strikingly different for those stars with and without atmospheric hydrogen. For the former group (seven program stars) the average is only 3.8, but 11.7 for the rest.

6. Conclusion

Spectral analyses of Wolf-Rayet stars require rather elaborate models of the non-LTE radiation transfer in expanding atmospheres. Although considerable progress has been achieved, these models cannot yet reproduce the observed spectra with the same accuracy as usual for static stars. While first model generations were restricted to the relatively simple elements helium and hydrogen, now very complex atoms like nitrogen can be accounted for as well. In the present paper we have applied those models comprehensively to the sample of Galactic WN stars. This allows to exploit the information contained in the nitrogen line spectrum.

The agreement between theoretical and observed spectra is generally good, thus basically confirming the "standard model" assumptions. However, characteristic discrepancies are also encountered. Partly we attribute these problems to deficiencies within the standard model, such as imperfect model atoms (e.g. the limited number of levels, inaccurate cross sections, or the approximative treatment of dielectronic recombination processes), and the neglection of metal line blanketing. The latter problem will be overcome by the next generation of models which is presently under construction. The non-predicted, but observed occurrence of weak lines from low ions (He I, N III) in WNE spectra probably indicates "clumping", i.e. the violation of the homogeneity assumption of the standard model. The best we can do at present is to neglect these low-ion lines for the analyses, as we have done in the present study. By neglection of clumping the mass-loss rates might be over-estimated by a factor between two and six, typically (Schmutz 1997, Hamann et al. in prep.), while the influence on the other parameters is probably small.

The parameters obtained from our new analyses of the nitrogen lines confirm the previous results from the helium analyses, as far as late subtypes (WNL) and early subtypes with strong lines (WNE-s) are concerned. For early subtypes with weak lines (WNE-w), however, the effective temperatures are considerably higher than previously thought. This implies much higher luminosities for the WNE-w subclass.

Most important, we do not find any longer that there are WN stars with luminosities below $10^{5.0}\, L_\odot$, contrary to the previous helium analyses (Papers I and II) in which 13 stars (two WNE-s, 11 WNE-w) fell below this threshold. This reduces the contradiction with the standard evolutionary calculations, as demonstrated with Fig. 9. The existing tracks for initial masses of 40 $M_\odot$ and 25 $M_\odot$ suggest that an (imaginary) track for about 30 $M_\odot$ might match well the average WNE luminosities, if that track returns to the blue side and does not ignite the SN explosion in the red supergiant regime.

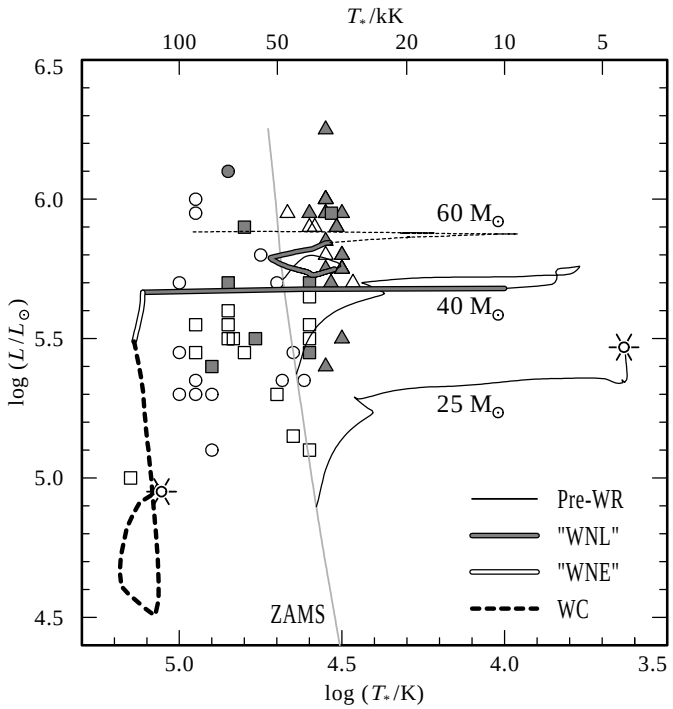

Fig. 9. Hertzsprung-Russell Diagram. Discrete symbols indicate the locations of the Galactic WN stars as obtained from our analyses. Triangles, circles and squares refer to WNL, WNE-s and WNE-w stars, respectively, while filled or open symbols indicate whether hydrogen has been detected or not. The theoretical tracks for initial masses of 25 $M_\odot$ and 40 $M_\odot$ (labels) are taken from Schaller et al. (1992) (metallicity $Z = 0.020$, their "$2 \times \dot{M}$" set). The evolutionary stages are indicated by different drawing styles (see inlet). Note that the subclass definitions "WNL" and "WNE" used here refer to the presence or absence of hydrogen at the surface. For 60 $M_\odot$ we display the first part of the alternative track from Langer et al. (1994) from the ZAMS through a first "WNL" stage to the LBV instability (thin-dashed).

Remaining problems concern the surface abundances. Note that the subclass definitions "WNL" and "WNE" used here refer to the presence or absence of hydrogen at the surface and thus can be directly compared with the representation of the observed stars by filled or open symbols. The effective temperatures can not be compared unambiguously, because the hydrostatic core radius is not an observable quantity.

For the most luminous WNL stars, the standard scenario does not predict the observed high hydrogen abundances (cf. Paper II), and alternative tracks with special mass-loss and/or mixing assumptions are more likely. In Fig. 9 we display the first part of the alternative track from Langer et al. (1994) for 60 $M_\odot$. This scenario adopts violent mass-loss when the star encounters (theoretically predicted) strange-mode instabilities. The star reaches a first WNL phase (with still plenty of hydrogen in its atmosphere) before becoming a luminous blue variable (LBV).

References

Cardelli J. A., Clayton G. C., Mathis J.S., 1988, ApJ Letters 329, 33
Crowther P.A., Hillier D.J., Smith L.J., 1994, A&A 293, 172
Crowther P.A., Hillier D.J., Smith L.J., 1995a, A&A 293, 403
Crowther P.A., Smith L.J., Hillier D.J., Schmutz W., 1995b, A&A 293, 427
Crowther P.A., Smith L.J., Hillier D.J., 1995c, A&A 302, 457
Hamann W.-R., 1994, Space Science Reviews 66, 237
Hamann W.-R., Schmutz W., Wessolowski U., 1988, A&A 194, 190
Hamann W.-R., Koesterke L., Wessolowski U., 1993, A&A 274, 397 (Paper I)
Hamann W.-R., Wessolowski U., Koesterke L., 1994, A&A 281, 184
Hamann W.-R., Koesterke L., Wessolowski U., 1995a, A&A 299, 151 (Paper II)
Hamann W.-R., Koesterke L., Wessolowski U., 1995b, A&AS 113, 559
Heger A., Langer N., 1996, A&A 315, 421
Hillier D.J., 1987a, ApJ Suppl. 63, 947
Hillier D.J., 1987b, ApJ Suppl. 63, 965
Hillier D.J., 1988, ApJ 327, 822
Hillier D.J., 1990, A&A 231, 116
Hillier D.J., Miller D.L., 1998, ApJ (in press)
van der Hucht K.A., Conti P.S., Lundström I., Stenholm B., 1981, Space Sci. Rev. 28, 227
van der Hucht K.A., Hidayat B., Admiranto A.G., Supelli K.R., Doom C., 1988, A&A 199, 217
Koesterke L., Hamann W.-R., Schmutz W., Wessolowski U., 1991, A&A 248, 166
Koesterke L., Hamann W.-R., Kosmol P., 1992, A&A 255, 490
Langer N., 1989, A&A 210, 93
Langer N., Hamann W,-R., Lennon M., Najarro F., Pauldrach A.W.A., Puls J., 1994, A&A 290, 819
Lundström I., Stenholm B., 1984, A&AS 58, 163
Schaller G., Schaerer D., Meynet G., Maeder A., 1992, A&AS 96, 269
Schmutz W., 1997, A&A 321, 268
Schmutz W., Hamann W.-R., Wessolowski U., 1989, A&A 210, 236
Seaton M.J., 1979, MNRAS 187, 73P
Smith L.F., 1968, MNRAS 140, 409
Smith L.F., Shara M.M., Moffat A.F.J., 1996, MNRAS 281, 163
Wessolowski U., Schmutz W., Hamann W.-R., 1988, A&A 194, 160